

Speciation and Mobility of Arsenic in Agricultural Lime

Gerald T. Schmidt, Ka Hei Lui, and Michael Kersten* Johannes Gutenberg University

Agricultural liming materials are used to correct soil acidity and to improve plant growth and microbial functionality. A relatively low-grade agricultural lime was found to contain up to 125 mg kg⁻¹ arsenic (As), which is above any fertilizing materials code threshold. The color of the milled material is brown due to amorphous dendrites. Microprobe elemental maps confirmed that these accessory oxide mineral phases are responsible for the elevated As concentrations in the limestone. The black Mn-bearing dendrites contain minor amounts of As, whereas the brown Fe-bearing dendrites contain the major part of the As inventory, with an Fe/As molar ratio around 100. Because the elemental maps represent only a few sample regions of interest (ROI), the results are corroborated by a bulk five-step sequential extraction of the lime, which suggests that a majority of the As is bound to acid-reducible phases. Because repartitioning of the As oxyanion during extraction cannot be ruled out, X-ray absorption spectroscopy with micrometer resolution (μ -XAS) was used as a solid-state speciation analysis approach. The μ -XAS results at the Fe K-edge for the selected ROIs revealed the brown dendrites to consist of ferrihydrite and goethite, whereas those at the As K-edge revealed that the pentavalent As species arsenate predominates, with As-Fe distance and coordination indicating binding as a mononuclear inner-sphere adsorbate complex. Batch experiments with soil exposed to submerged conditions of up to 41 d revealed a negligible As release rate from the lime (approximately 40 ng kg⁻¹ d⁻¹). The results of this study corroborate regulatory codes that set the permissible As content in agricultural lime relative to the respective Fe content.

GRADUAL increases of many trace element concentrations in agricultural soils over the past decades have led to concerns regarding potential toxicological implications and detrimental long-term trends. An improved understanding of the mobility and bioavailability of trace elements introduced during agricultural activities is, therefore, relevant to identify potential risks and to establish effective legal limits. Lime amendment is routinely applied on croplands to improve yields by optimizing soil acidity, cation exchange capacity, and microbial functionality (ALA, 2008a). Soils differ considerably in their pH, and most temperate crops grow best when soil pH is approximately 6.5 to 7.0. For many centuries, lime in various forms has been used to raise soil pH and thereby improve soil fertility. Lime is applied to land in quantities larger than any other inorganic material (typically 2–10 t ha⁻¹), and liming is widely practiced as a regular feature of every crop rotation. In Germany, about 1.5 million dry tons of lime are used annually for forestry and agriculture (FGALI, 2008). Lime is usually produced from natural rock (i.e., mined in limestone, dolomite, or chalk quarries) and is finely pulverized before use. Because large quantities of liming materials are required per unit of land and because these materials are low-value, high-bulk products, it is important to find local sources to keep transportation costs reasonably low even if the local limestone is of low grade. Crystalline metamorphosed limestone usually contains minor oxide impurities, often in the form of decorative dendrites. “Low grade” means that abundant Fe and Mn oxides may confer to the bulk rock a brownish-yellow color, which may diminish its worth for building material but not necessarily as a fertilizer. Concentrations of metals in liming materials are commonly low and far from exceeding threshold values (McBride and Spiers, 2001). However, given the known affinity of Fe and Mn oxides to scavenge toxic trace metals and metalloids, specific cases with exceptionally high oxide contents are worth investigating to assess potential risks of soil and ground water contamination by these bulky amendments.

The amount of heavy metals being incorporated even with repeated applications may be negligible compared with that present in the volume of receiving soil. However, if coupled with water-

Copyright © 2009 by the American Society of Agronomy, Crop Science Society of America, and Soil Science Society of America. All rights reserved. No part of this periodical may be reproduced or transmitted in any form or by any means, electronic or mechanical, including photocopying, recording, or any information storage and retrieval system, without permission in writing from the publisher.

Published in *J. Environ. Qual.* 38:2058–2069 (2009).
doi:10.2134/jeq2008.0441
Received 6 Oct. 2008.

*Corresponding author (kersten@uni-mainz.de).

© ASA, CSSA, SSSA
677 S. Segoe Rd., Madison, WI 53711 USA

G.T. Schmidt, K.H. Lui, and M. Kersten, Environmental Geochemistry Group, Institute of Geosciences, Becherweg 21, Johannes Gutenberg-Universität, 55099 Mainz, Germany. G.T. Schmidt, present address: Karl Winnacker Institute, Dechema e.V., Theodor-Heuss-Allee 25, 60486 Frankfurt am Main, Germany.

Abbreviations: ALS, Advanced Light Source; E₀, edge energy in a X-ray absorption spectroscopy energy scan; EPMA, electron probe X-ray microanalysis; EXAFS, extended X-ray absorption fine structure spectroscopy; HG-AAS, hydride generation atomic absorption spectrometry; N, coordination number of EXAFS scattering path shells; ROI, region of interest; RSF, radial structure function; XANES, X-ray absorption near-edge structure; XAS, X-ray absorption spectroscopy; XRD, X-ray diffractometry; XRF, X-ray fluorescence spectroscopy; σ^2 , Debye Waller Factor of EXAFS scattering path shells.

logged conditions as a worst case, redox-sensitive manganese oxides could become reduced and release plant-available Mn^{2+} species as a result of microbial respiration, which can cause Mn toxicity in sensitive plants. Little is known about the behavior of the limestone oxide impurities in such reactions, and in particular about toxic trace elements such as arsenic (As), which are known to be accumulated in the oxides. The introduction of dendrite-bearing limestone to such environmental conditions could exacerbate the problem in the longer term as metals become mobilized during reduction of the oxide dendrites.

The mobility and chemical association of metals in soil samples are commonly elucidated using wet-chemical sequential extraction of the various metal-bearing phases. However, this approach presents serious limitations due to artifacts (for a review, see Kersten, 2001). In the conventional sequential extraction methods, undesirable chemical side reactions may render the results disputable. Arsenic associated with amorphous iron oxides, for example, is not necessarily released into solution after reductive dissolution due to readsorption onto other minerals unaffected by the chosen extractant (Hudson-Edwards et al., 2004). Synchrotron-based X-ray absorption spectroscopy (XAS) has, in recent years, emerged as a tool with proven capability for speciation analysis of toxic trace elements, such as As in natural ferromanganese oxides (Waychunas et al., 1993; Manceau, 1995; Fendorf et al., 1997; Sherman and Randall, 2003; Marcus et al., 2004; Cancès et al., 2005). By being nondestructive, it preserves the chemical integrity of the sample and provides for detailed chemical speciation analysis on a molecular level. For improvement of credibility of the results, a combination of several analytical techniques was used. The purposes of the present study were (i) to detect the main host phase(s) of As in agricultural lime samples, (ii) to analyze its valence state and binding form by solid-state speciation X-ray analysis, and (iii) to assess its potential mobility on amendment in soil, especially under high phosphate load or waterlogged conditions. The results from the conventional soil fractionation/incubation experiments and solid speciation analysis provide a sound basis for evaluating existing regulation codes for agricultural lime.

Materials and Methods

Study Area

Limestone samples were derived from a quarry in the Permian-Triassic sedimentary rock complex of the Spessart region, Germany (Suppl. Fig. S1). The Mg-bearing limestone classified as Zechstein dolomite has been exploited for over a century. One of the most obvious features of this limestone is the frequent black and brown oxide dendrites found in fractures and on plate surfaces, mostly in thin layers, and in veins and plaques. The source of the dendrite mineralization is likely stratabound metal-rich shale ("Kupferschiefer") in the underlying stratigraphic bed related to post-Variscan hydrothermal activity that affected the Spessart area in Middle Jurassic to late Early Cretaceous. Metal-bearing solutions penetrating NE-SW striking faults in the vicinity of the limestone quarry have led to base-metal mineralization exploited in the past by two small copper, lead, and silver

mines, known also for a variety of As-bearing minerals (Schmitt, 2001; Okrusch et al., 2007). The main commercial product of the quarry is ground Carbonatic Magnesium Lime 85, samples of which were acquired in a manner consistent with consumer purchase for agricultural use. The specifications according to the producer's information are: 60% $CaCO_3$ and 25% $MgCO_3$, ground to a powder of grain size <3 mm (97%) and <1 mm (70%). Its relatively dark brown color is due to the presence of Fe/Mn oxides, which is more than most commercially produced limestone powder would have.

A representative surface sample (0–20 cm) of clayey soil (Dystric cambisol) morphologically typical of the German highland region was collected from a forest location west of Wiesbaden (Suppl. Figure S1). This site pertains to the unamended acidic soils of the quaternary terrace sequence, which form part of the foreland of the Taunus hills. Agricultural activities in this area include winegrowing, market gardening, and fruit growing. Any organic debris at the surface was manually removed. The soil sample used for the incubation batch experiments had an original pH of 4 and an organic carbon content of 4% (dry w/w). The soil sample was air-dried and sieved to pass a 2-mm sieve before being subdivided for the batch experiments. The soil samples used for the incubation experiments yielded the following element concentrations in microwave HCl digestion analyses: As, 8 ± 0.9 mg kg^{-1} ; Fe, 14.9 ± 3.0 g kg^{-1} ; and Mn, 0.68 ± 0.07 g kg^{-1} .

Wet Chemical Digestions

For the chemical characterization of lime and soil with respect to the background contents of the elements pertinent for this study, subsamples were dissolved by microwave digestion with HCl (32%) in closed polytetrafluoroethylene containers. Subsamples from a range of six different specimen bags of limestone powder provided by the producer were milled to a fineness of 400 mesh using an agate mortar and pestle and digested by the same procedure. An anionic, P-based, sequential extraction scheme had been developed specifically for As fractionation (Keon et al., 2001). In its original form, it includes eight extraction steps, but only five of them were deemed relevant: (i) treatment with 1 mol L^{-1} NaH_2PO_4 (pH 5) for 24 h at 25°C to remove strongly adsorbed As, (ii) treatment with diluted 1 mol L^{-1} HCl for 1 h at 25°C to dissolve carbonates and amorphous Mn hydroxides, (iii) 0.2 mol L^{-1} NH_4 -oxalate/oxalic acid (pH 3) for 2 h at 25°C in darkness to dissolve poorly crystalline Fe/Mn hydroxides, (iv) 0.05 mol L^{-1} Ti(III)-citrate EDTA bicarbonate (pH 7) for 2 h at 25°C to dissolve crystalline Fe hydroxides, and (v) microwave digestion with HCl (32%) for any residual fraction. Nitric acid was not used because it interferes with the iodide pre-reduction step in hydride generation-atomic absorption spectrometry (HG-AAS) used to measure As concentrations. The pH was monitored in the first two extraction steps to ensure that the carbonate content did not exceed the buffer capacity. It was not necessary to adjust the pH at the chosen solid/solution ratio of 1:100. An orbital shaker instead of an end-over-end shaker was used to prevent material blow-out due to CO_2 overpressure. The reagent used in step 4 was produced following

the recommendations for the extraction of crystalline Fe oxides by Ryan and Gschwend (1991). The TiCl_3 solution used to prepare this extraction reagent is hazardous and should be handled with caution, preferentially under a N_2 -filled glove bag. In step 5, the residue was transferred to polytetrafluoroethylene tubes for microwave HCl digestion and analytical yield control. A solid residual was left over from all digestions. Supernatants were separated on centrifugation and subsequent filtration by 0.2- μm membranes and acidified by HCl.

For quality assurance/quality control, three subsamples of a certified reference material (GBW07108/GSR-6, a commercial certified reference material limestone sample from China with As content of $4.7 \pm 0.9 \text{ mg kg}^{-1}$) were treated identically. The total As concentrations of all samples were measured in triplicate using wavelength-dispersive X-ray fluorescence analysis (MagiX PRO; Philips, The Netherlands; As detection limit 1 mg kg^{-1} for powder pellets). The concentration of dissolved As was determined using a hydride generator coupled to an atomic absorption spectrometer (HG-AAS) (VGA 76; Varian, Palo Alto, CA). To determine the amount of any As^{3+} present, the iodide pre-reduction step was left out, and 0.1 mol L^{-1} citric acid was used in the hydride generator (Maity et al., 2004). The detection limits were $0.4 \mu\text{g L}^{-1}$ (total As) and $1 \mu\text{g L}^{-1}$ (As^{3+}). The recovery rate of As was assessed at $100 \pm 20\%$ on average ($\pm \text{SD}$) by comparison of the sum of all extraction steps, the single HCl (32%) digestions, and the X-ray fluorescence spectroscopy (XRF) analysis yields, even for the certified reference material with 4.7 mg kg^{-1} As. Dissolved transition metals like Fe may interfere in the determination of As by HG-AAS (Aggett and Hayashi, 1987). Interferences by the enhanced Fe concentrations led to higher apparent As recovery rates in all but the first extraction step if no masking reagents, such as cysteine or the standard addition mode, were used, according to a recommendation by Näykki et al. (2001) (Suppl. Fig. S2). The concentration of dissolved Fe and Mn was determined by conventional flame atomic absorption spectrometry (Varian SpectraAAS 300), with detection limits of 0.5 mg L^{-1} (Fe) and 0.1 mg L^{-1} (Mn).

Laboratory-based X-ray Analyses

To characterize the mineral phases of impurities in the limestone, samples of black oxide plaques and brown dendrites scraped off the rock surface and the residue of the first extraction step were analyzed by X-ray powder diffractometry (XRD). Several known crystalline Fe and Mn oxide minerals were measured as reference substances. The XRD was recorded using a Seifert XRD 3000 TT diffractometer, $\text{Cu K}\alpha$ radiation, 0.03° in 2θ intervals, and a 2-s dwell time/step. The irradiated sample surface was kept constant using an automatic divergence slit. The commercial software package RayfleX (Seifert, Germany) with the PDF2 database was used for phase identification.

A piece of flat rock surface with predominantly brown and relatively few black dendrites was analyzed by electron probe X-ray microanalysis (EPMA) using a JXA 8900 RL microprobe (Jeol, Japan) with a beam of 20 kV/50 nA. The sample was selected for its dense coverage with dendrites (i.e., the highest available concentration of impurities) on which the analyses were focused. Because polishing

would have removed the thin dendrite coatings, the surface was not as smooth as necessary for quantitative analyses. Regions of interest (ROIs) were selected under an optical microscope and screened by the fast energy-dispersive channel for their element composition. High-spatial-resolution ($1.5 \mu\text{m}$ per pixel) elemental maps were then recorded from three Fe- and Mn-rich ROIs using the wavelength-dispersive channels for Ca, Fe, Mn, and As.

Synchrotron-based X-ray Analyses

The same dendrite-coated limestone sections were used for in situ $\mu\text{-XRF}$ and $\mu\text{-XAS}$ at the Berkeley Advanced Light Source (ALS) beamline 10.3.2. The rather limited beamtime for this study made a selection of the ROI necessary based on $\mu\text{-XRF}$ maps. The maps were recorded at 13 keV using a pixel size of $20 \times 20 \mu\text{m}^2$; a dwell time of 50 ms per pixel; and a scanning speed of $400 \mu\text{m s}^{-1}$ for As, Fe, and Mn distributions. Three Fe- and As-rich spots were selected for $\mu\text{-XAS}$ based on the previous area mapping by $\mu\text{-XRF}$. Harmonic rejection was achieved by detuning the Si(111) double crystal monochromator to 50% of the rocking curve maximum. X-ray absorption spectroscopy energy scans were done at the Fe K-edge (7112 eV), with two repetitions each, and at the As K-edge (11867 eV), with up to seven repetitions at ambient temperature in fluorescence mode using a seven-element Ge detector. Energy calibration was achieved to a precision of 0.1 eV by using the known position of monochromator glitches.

Bulk spectra of the As reference mineral scorodite ($\text{FeAsO}_4 \cdot 2\text{H}_2\text{O}$) were measured at Hamburg Synchrotron Laboratory beamline A1 in transmission mode (Suppl. Fig. S3 and Suppl. Table S1). The pulverized sample was pressed to a homogeneous pellet using polyethylene powder as a binder. Energy scans were done at the As K-edge under vacuum at ambient temperature using ionization chamber detectors. X-ray absorption spectra for reference Fe oxides from previous studies were also used for this study (Marcus et al., 2004). Spectra averaging and deglitching were done using WinXAS (Ressler, 1998) and the LabView software provided at ALS beamline 10.3.2. The Athena/Artemis software packages (Ravel and Newville, 2005) were used for background subtraction, normalization, extraction of extended X-ray absorption fine structure spectroscopy (EXAFS) functions $\chi(k)$, Fourier Transformation, and parameter fitting. The Fourier transformation of averaged EXAFS spectra was performed by applying a Kaiser Bessel window with the window parameter 4. A k -window between 2.5 and 12 \AA^{-1} was chosen for the Fe K-edge and between 2 and 12 \AA^{-1} for the As K-edge spectra fitting. The Atoms and FEFF (Rehr and Albers, 2000) codes integrated in Artemis software package were used for calculating theoretical scattering paths and fitting to selected peaks in the radial structure functions (RSF). A theoretical atomic cluster model of scorodite (Kitahama et al., 1995) was used for FEFF parameter fitting (Table 1). The fitting procedure (Artemis software) was done in the R-window 1 to 4 \AA for the k -weights 2 and 3 simultaneously. The value of the shift in edge energy in an X-ray absorption spectroscopy energy scan (E_0) was also determined from this scattering path ($\Delta E_0 = 8.5 \text{ eV}$) and then fixed for all other fits. Independent shifts ΔR of the scattering path

length were assumed for each shell. The Debye Waller Factor σ^2 of the As-O shell was determined from the fit after fixing the coordination number $N = 4$. The σ^2 of the As-Fe shells was initially set to the value derived from the fit of scorodite while the coordination numbers were kept floating, and then the resulting N were fixed and σ^2 was determined from the fit. The best fit (i.e., the lowest r factor) was achieved once the thus optimized σ^2 was fixed, and the coordination numbers N were floated. The many-body amplitude reduction factor was fixed at 1.0 during all fits.

Incubation Batch Experiments

Lime (in terms of CaO) demand of the soil sample was determined according to the German standard (VDLUFA, 1991), which is comparable to the recommendations published by ALA (2008b). The buffer capacity was estimated by measuring the pH in CaCl_2 and in Ca acetate suspension. The lime demand was then taken from the respective VDLUFA table in which the ΔpH value is weighted according to the soil texture, the organic carbon content, and the target pH. The resulting lime demand was at minimum 700 g m^{-2} for a soil depth of 20 cm. This amount was converted to the actual CaCO_3 content of the limestone sample, which yielded an amendment at a rate of 10 g kg^{-1} dry soil. As a worst-case scenario, high liming experiments were prepared with 100 g lime per kg soil. For comparison, equivalent samples were prepared with analytical grade CaCO_3 (Merck p.a. quality). As many as 12 subsamples of each type of lime addition were prepared. There were 12 untreated (control) samples.

Soil subsamples of 30 to 35 g (DW) each were saturated (35% w/w) with a $1.0 \text{ mmol L}^{-1} \text{ CaHPO}_4 \cdot 2\text{H}_2\text{O}$ (p.a. quality) solution in deionized water and incubated in 50-mL centrifuge tubes, which were kept capped at ambient room temperature (around 20°C). The pH and redox potential in the soil pore water were monitored, and pore water was extracted from four samples of each type after 1, 20, and 41 d by centrifugation ($3300 \times g$, 30 min) and subsequent membrane filtration ($0.2 \mu\text{m}$). The amount of extractable pore water was somewhat less than previously added and varied from 2 to 7 mL. For calculation of As mobilization rates, the water content of each sample was determined after centrifugation by weighing extracted pore water as well as wet and dry remaining soil material. No significant loss of water through evaporation was observed over the incubation period. No attempt was made to determine the amount of colloids $<0.2 \mu\text{m}$ in the filtrates, but care was taken to avoid contact with ambient air by applying argon during filtration to prevent oxidation and oxide colloid precipitation. The filtrates were stabilized by HCl acidification ($\text{pH} < 2$) according to a recommendation by McCleskey et al. (2004) and stored in darkness at 4°C for 1 d until they were analyzed for As concentration and speciation as detailed previously. Analytical results were obtained for each replicate separately, and then average and SD values were calculated.

Results and Discussion

Wet Chemical Analyses

Total acid (HCl) digestion of the six different lime charges yielded bulk Fe, Mn, and As concentrations of $8.5 \pm 2.2 \text{ g kg}^{-1}$,

Table 1. Parameters resulting from the FEFF fit of scorodite crystal structure data to the As bulk extended X-ray absorption fine structure spectroscopy spectra from scorodite ($\Delta E_0 = 6.94 \pm 1.37 \text{ eV}$; r factor = 0.046). The highest correlations were found between the path lengths of As-O(2) and As-Fe (-0.88) and between the path length of As-O(1) and ΔE_0 (0.79).

Scattering path	N	σ^2	R
			\AA^2
As-O(1)	4.0	0.0020 ± 0.0003	1.69 ± 0.005
As-O(2)	2.0	0.0020 ± 0.0003	3.34 ± 0.098
As-Fe	2.0	0.0022 ± 0.0021	3.37 ± 0.022

$5.9 \pm 1.8 \text{ g kg}^{-1}$, and $62 \pm 12 \text{ mg kg}^{-1}$, respectively (average of five subsamples). A sixth sample with excessive 125 mg kg^{-1} As was not considered for averaging and indicates inhomogeneities in lime composition. Nonetheless, the As content in all charges is above the global mean of 2.6 mg kg^{-1} for limestone (Baur and Onishi, 1969) or the 2 to 4 mg kg^{-1} for pelleted limestone commonly used in soil amendment (McBride and Spiers, 2001; Price and Pichler, 2006) and even higher than the values of 10 to 16 mg kg^{-1} that are typical for phosphate fertilizers (Charter et al., 1995; Raven and Loeppert, 1997). Direct XRF analyses of all lime samples (including the reference limestone) yielded 25% higher bulk Fe ($11.3 \pm 2.6 \text{ g kg}^{-1}$) and Mn ($7.4 \pm 2.2 \text{ g kg}^{-1}$) concentrations, probably because of HCl-insoluble residual Fe/Mn-bearing minerals like silicates. However, these residual phases do not host a significant portion of As because no such mismatch between both analyses was found for this element ($66 \pm 14 \text{ mg kg}^{-1}$). Nonetheless, it is unclear whether the As enrichment is hosted by the carbonate matrix as reported recently for the case of quaternary lacustrine travertine deposits in Tuscany, Italy (Di Benedetto et al., 2006) or by the dendrite impurities. A common approach to elucidate the As partitioning was to apply the sequential extraction scheme on the samples.

The results of the sequential extraction analyses are shown in Fig. 1. An As proportion of on average $18 \pm 4\%$ was mobilized by the first phosphate step. Assessing the stability of the As pool in the lime against desorption by phosphate would mimic a rather realistic field situation. Mineral surface-adsorbed arsenate may be mobilized in competition with phosphate because of the smaller size and higher charge density of the latter oxyanion (Manning and Goldberg, 1996; Keon et al., 2001). The proportion exchangeable during this first step does not increase with total extractable As and is relatively low in comparison to literature data (Fig. 2). Cai et al. (2002), for example, found up to 80% of the total As to be exchangeable in the fine fraction of golf course soils. However, desorption of As even by concentrated phosphate extractants ($0.5\text{--}1 \text{ mol L}^{-1}$) seems to depend on the type of the sorbent, in particular its crystallinity, and on the residence time of the As (Pigna et al., 2006). Geological residence time and sorbent crystallinity is clearly high in the limestone samples, and the relatively low amount extractable by $1 \text{ mol L}^{-1} \text{ NaH}_2\text{PO}_4$ could therefore be due to the formation of stabilized As rather than a lack of As sorbing phases.

Negligible amounts of the potential Fe and Mn sorbate phases were dissolved by this first step (both $<4\%$), but 25% of the total Fe and 42% of Mn were dissolved in the second

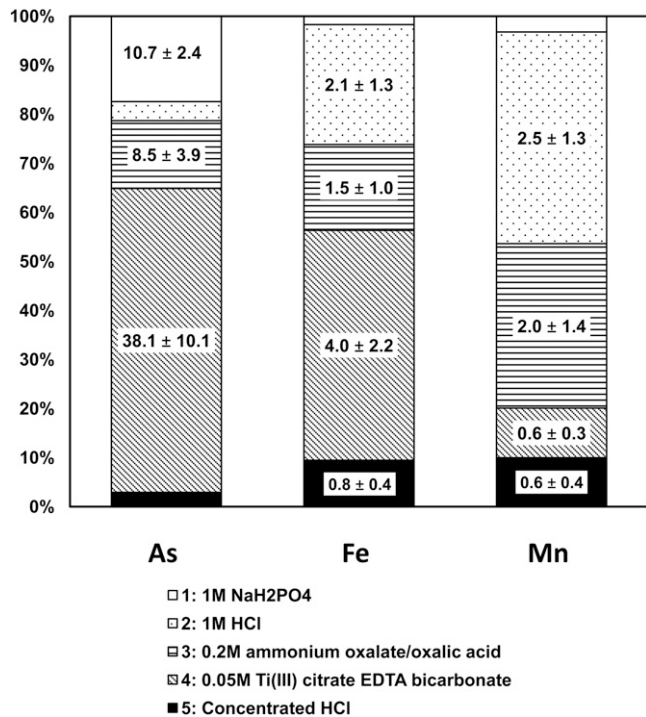


Fig. 1. Bar chart of sequential extraction results in terms of relative proportions of the five steps. Arsenic concentrations (dry w/w \pm SD) are displayed within the related bar stacks as an average of five samples.

1 mol L⁻¹ HCl-soluble step. Because the original valences of these elements are not known (Fe(II) or Fe(III) and Mn(II) or Mn(IV), respectively), it is not possible to designate the extraction yield as a carbonate or as an amorphous oxide species. However, a negligible fraction of As (<3%) was found in this second step. The dark brown residue deliberated from the carbonate matrix by this extraction step yielded the following average concentrations (on microwave digestion analyses of separate subsamples): Fe, 89 \pm 1.7 g kg⁻¹; Mn, 26 \pm 0.3 g kg⁻¹; and As, 940 \pm 80 mg kg⁻¹. It clearly hosts the majority of the total As. The third moderately acid-reducing extraction step dissolved from this residue an additional 18% Fe, 33% Mn, and 14 \pm 5% of the total As contents. In the fourth strongly reducing step, 46% of the total Fe content and 61 \pm 6% of the total As were dissolved, with a molar ratio As/Fe = 1.1 \times 10⁻². The amount of Mn mobilized in this step is very small (<1 g kg⁻¹). This indicates that crystalline Fe oxides dominate this fraction. The last step dissolved an additional 9% of the Fe content and negligible fractions of As and Mn (<3%). There is a non-dissolved residual portion of 25% of Fe and Mn, but no As was left over after this step compared with the sum released in all extraction steps with bulk solid analyses by XRF as mentioned above.

The results suggest that As bounds to oxide phases of the dendrites rather than to the carbonate matrix. Moreover, the majority of the reducible As fraction is bound to crystalline Fe oxides. A lower proportion is mobilizable in steps 2 and 3, which suggests a binding to Mn oxides or less crystalline Fe oxides. However, this As fraction might be higher because re-adsorption

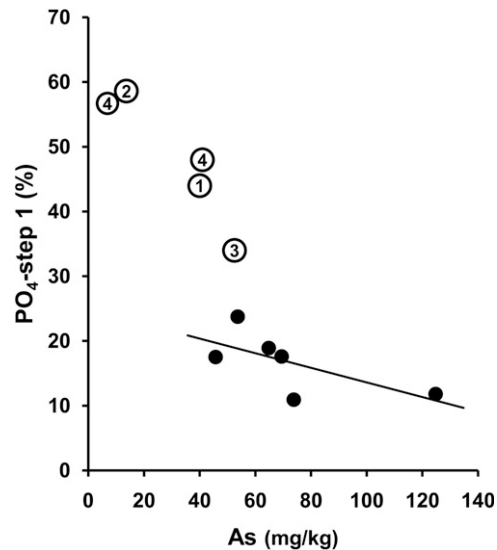


Fig. 2. Percentage of As extracted in the first PO₄ step against the total As concentration. The open dots refer to data selected from literature: (1) river sediment (Keon et al., 2001), (2) fine fraction of golf course soils (Cai et al. 2002), (3) river bank deposits (Eiche et al., 2008; Berg et al., 2008), and (4) tin mine-affected paddy field soils (Ngoc et al., 2009).

of released metals is a common artifact in sequential extraction analysis, as long as potential sorbents are not exhausted (Gruebel et al., 1988). Because arsenate oxoanions are readsorbed even under moderately acid-reducing conditions (Jackson and Miller, 2000), it could not be clarified whether the As load on crystalline Fe oxide is the original binding form or whether it is artificially enhanced by the scavenging of As in previous extraction steps 2 and 3. Direct X-ray spectroscopic speciation analysis was deemed necessary to resolve these ambiguities in the interpretation of the wet chemical fractionation analysis.

X-ray Diffractometry and X-ray Fluorescence Spectroscopy Analyses

The XRD pattern of the black plaques is consistent with that derived from Harvard mineral reference sample no. 83928 for the crystalline Ba-bearing manganate mineral romanecchite (or Ba-psilomelane). This mineral is known from other studies to dominate Mn-rich rock dendrites (McKeown and Post, 2001). The XRD patterns of the brown dendrite material indicate multiphase composition dominated by quartz peaks (Suppl. Fig. S4), with only trace peaks of the two Fe hydroxides goethite and ferrihydrite. No trace of Fe/Mn carbonates was found, which rules out contribution of these phases to the Fe/Mn fraction dissolved in the second extraction step. No separate As phases could be detected by XRD, which was expected considering the As content of the plaques.

Figure 3a shows a representative ROI example of the many EPMA-generated element maps of Mn, Ca, Fe, and As. The distribution of As in this sample surface is heterogeneous but somewhat systematically predictable. A comparison of As concentrations in Fe/Mn-rich sites with that of pure limestone Ca sites reveals that As is enriched in the dendrite material

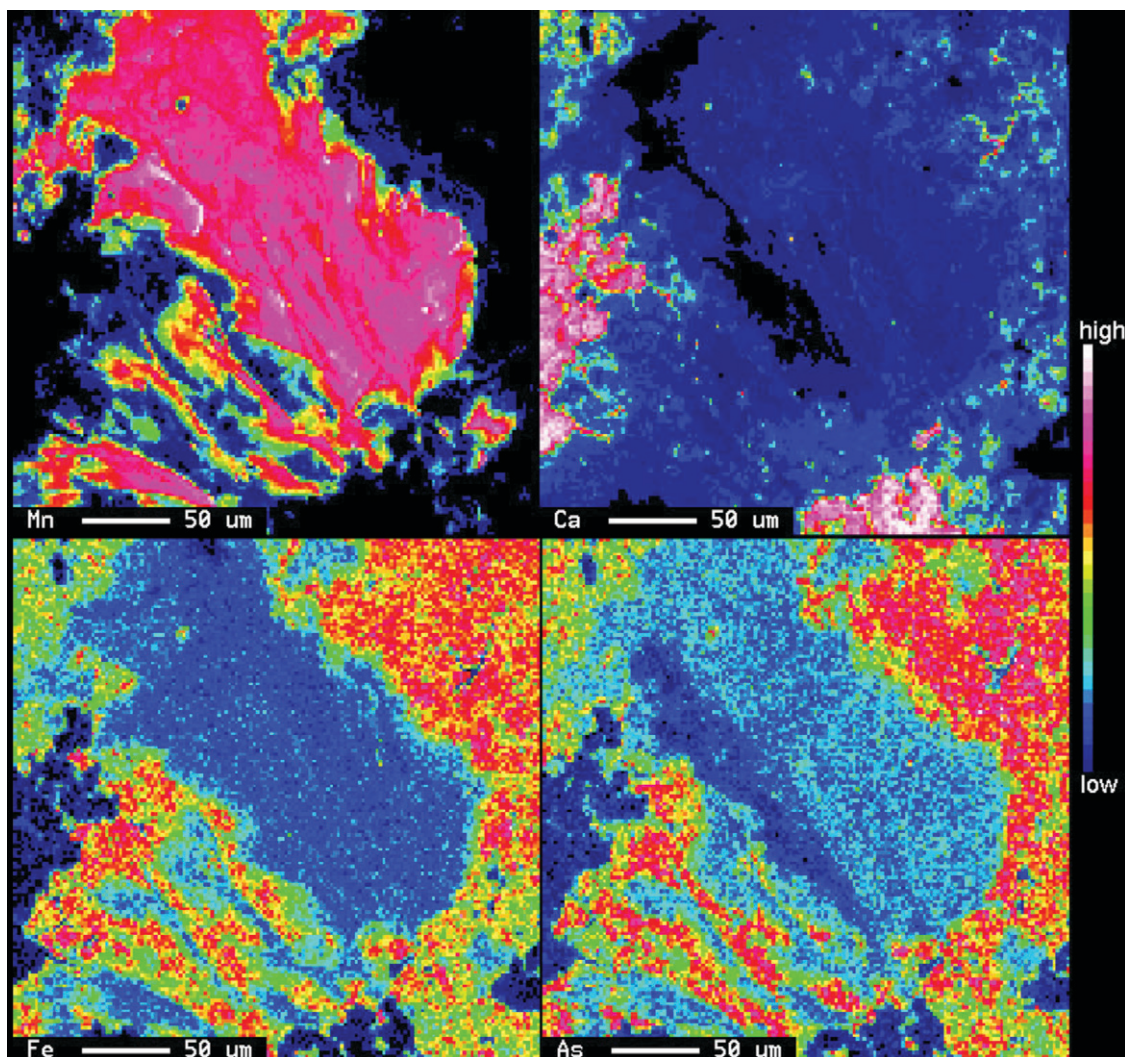


Fig. 3. (a) Electron probe X-ray microanalysis maps of the distribution of Mn, Ca, Fe, and As in a dendrite coating on a limestone sample.

rather than in the carbonate matrix. However, there is also a significant difference in As content of the discernible oxide phases. The center of the maps is covered by a Mn-bearing area with less As surrounded by a Fe-bearing area with higher As amount. In the lower left edge of the maps, there is an area of high Ca content without any dendrite, hence the lowest Mn, Fe, and As concentrations. The μ -XRF maps derived with another sample at the ALS synchrotron beamline show the same pattern of element distribution (Fig. 3b). Red areas in the tricolor map represent thin black Mn oxide dendrites, while the larger greenish areas represent the dominating brown Fe oxide dendrites, which also showed the highest As concentrations. A clear association of As with Fe-rich spots, and a less significant association with the Mn-rich spots, is evident from the spatial distributions, and, even more clearly, from the scatter plots shown in Fig. 3c. The XRF results thus confirm the sequential extraction results that Fe oxide (brown dendrites) is the dominant As-bearing phase in the limestone, with Mn oxide (black dendrites) being a distant second.

XAS Analyses

The As content in the limestone samples is environmentally relevant but low enough to preclude bulk As K-edge XAS analysis of reliable spectra quality. As-rich spots were therefore used for μ -XAS analysis selected from a representative μ -XRF elemental map (Fig. 3b, spots 1–3). They are rich not only in As but also in Fe (blue-green on the map), representing the dominating form of As bound in the limestone, in accordance with the findings of the wet chemical and EPMA analyses. The μ -XRF results and a comparison of single XAS spectra from all three spots led to the conclusion that they all consist of the same substance. The scans at the As K-edge were obtained first (seven repetitions on spot 1). To rule out any potential influence of beam damage, scans at the Fe K-edge were obtained at spot 1 and spot 2 (two repetitions each) and screened for differences (none was found).

The Fe K-edge XAS spectra obtained at spots 1 and 2 were averaged to improve the signal-to-noise ratio. The resulting X-ray absorption near-edge structure (XANES) spectrum is compatible with Fe^{3+} in octahedral coordination (Suppl. Fig.

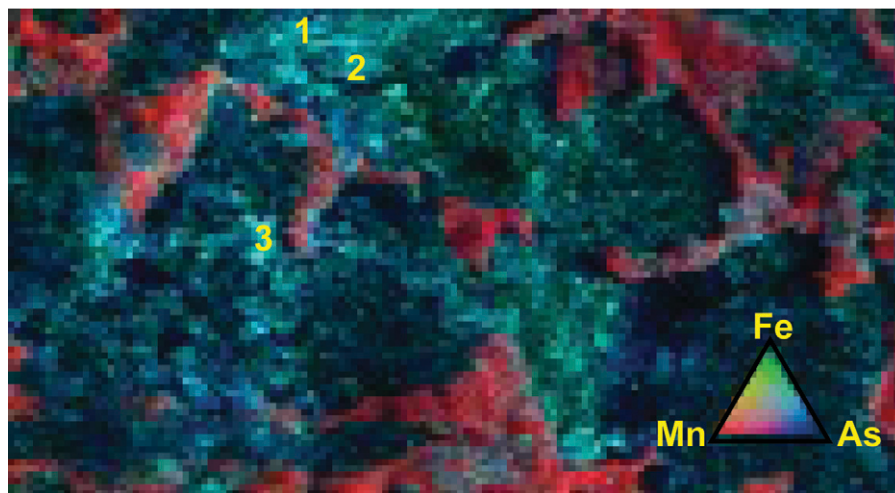


Fig. 3. (b) μ -X-ray fluorescence spectroscopy (μ -XRF) map of a dendrite area acquired at the ALS synchrotron beamline 10.3.2. Each pixel is colored according to the normalized fluorescence signals of Mn (red), Fe (green), and As (blue). The image area measures $2.36 \times 1.56 \text{ mm}^2$, and the pixel resolution is $20 \times 20 \text{ }\mu\text{m}^2$. The numbers encode the spots used in this region of interest for μ -X-ray absorption spectroscopy.

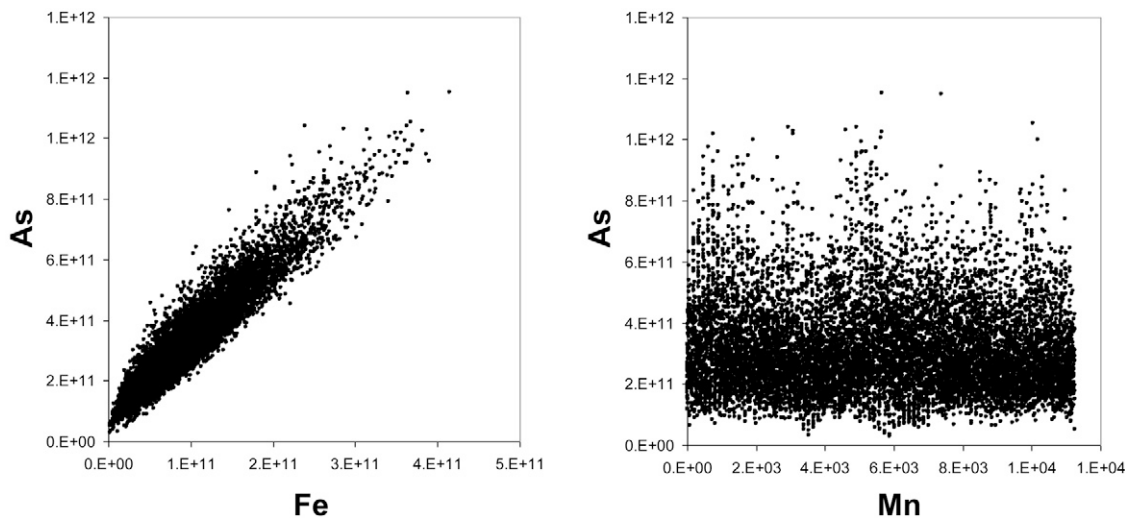


Fig. 3. (c) Scatter plots of Fe and Mn vs. As μ -XRF signals.

S5; Manceau and Gates, 1997). The averaged Fe K-edge EXAFS spectrum was fitted in k -space by calculating the weighted sums of reference spectra acquired at the same beamline earlier (Marcus et al., 2004) without normalizing their sums to 100%. Linear-combination fits of EXAFS data in k -space were done using Athena. Best fits were achieved using reference data of goethite and six-line ferrihydrite (Fig. 4). The brown dendrite fit yielded 61% goethite and 27% six-line ferrihydrite with a χ^2 of $\pm 21\%$. The goethite/ferrihydrite ratio of about 2 thus found in the dendrite surface samples indicates some predominance of the crystalline Fe oxide, although the error margin is so high that the shares between both phases could be also equal. The latter would be comparable with the sequential extraction results once the extracted Fe in steps 2 and 3 is assigned to ferrihydrite and the Fe in step 4 to goethite, which are of equal shares rather than a ratio of 2. Otherwise, the linear-combination fit result would suggest that part of the crystalline goethite is dissolved in the moderately acid-reducing steps 2 and/or 3.

The As K-edge XAS spectra obtained at spot 1 were averaged to improve the signal-to-noise ratio. The resulting XANES spectra (Suppl. Fig. S6, also including one spectrum from spot 3 for comparison) show an E_0 value (defined at halfway up the absorption edge jump) of $11,871.8 \pm 0.1 \text{ eV}$, which, together with the thin, steep, and high shape of the white line, indicates predominance of pentavalent As. Good EXAFS fits were achieved in k - and R -space by FEFF calculations using scorodite scattering paths as a structural reference (Fig. 5; Table 1). The high quality of the fit, even for the imaginary part of the Fourier transform, is corroborated by an overall low r factor of 0.017. The first RSF peak is characteristic for the O shell of the arsenate species with distance $R = 1.69 \text{ }\text{\AA}$ and coordination $N = 4$ (Waychunas et al., 1993). A reliable fit of the second shell peak in the RSF at $R > 2 \text{ }\text{\AA}$ was not possible by choosing only one As-Fe scattering path. The best fit was achieved using a Fe shell at $R = 2.74 \text{ }\text{\AA}$ ($N = 1.3$), a slightly higher coordinated second one at $R = 2.92 \text{ }\text{\AA}$ ($N = 1.9$), and a third one at $R = 3.57 \text{ }\text{\AA}$ with $N = 2.0$, all with a common σ^2 of $0.009 \text{ }\text{\AA}^2$ relative to the sec-

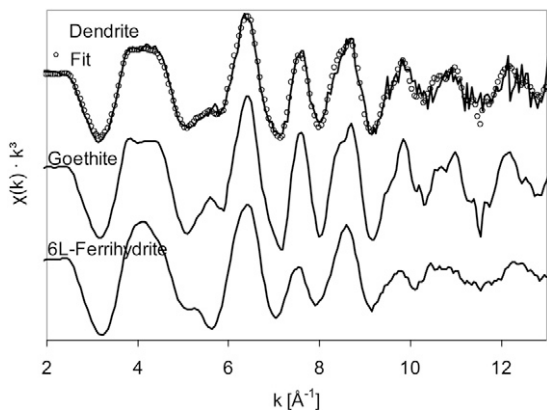


Fig. 4. Iron K-edge extended X-ray absorption fine structure spectroscopy $\chi(k) \times k^3$ functions of brown dendrite spots 1 and 2 in Fig. 3b and of reference samples goethite and 6L-ferrhydrite, respectively. Circles trace the linear-combination fitting curve.

ond shell of the scorodite model (Table 2). The inclusion of a multiple scattering path As-O-O-As at 3.10 Å had little effect (i.e., the r factor was reduced by 0.4%), and its contribution to the RSF is therefore insignificant. The shorter MS path (2.85 Å), as suggested by Sherman and Randall (2003) to interfere with As-Fe paths at 2.85 ± 0.10 Å, deviates considerably from the crystal structure model. FEFF calculation shows that only the As-O-O-As three-leg path has some intensity, with $R_{\text{As-O-O-As}} = 3.02$ to 3.10 for a typical AsO_4 tetrahedron. A length shorter than 3 Å would require a considerable distortion of the tetrahedral structure, which has not been reported. In fact, because the As-O bond is highly covalent, the oxyanion tetrahedra are rigid and cannot be easily deformed. Moreover, because $R_{\text{As-O}} = 1.7$ Å, a multiple scattering peak at 2.85 Å would imply an O-O distance of $(2.85 \times 2) - (1.7 \times 2) = 2.3$ Å. This is an almost impossibly short distance for an O-O pair. Attempts of fitting a model with a single As-Fe and the multiple scattering paths were also unsuccessful. The highest correlations were found between the σ^2 of the first and second As-Fe scattering paths (0.86) and between their path lengths (0.76).

The occurrence of more than one As-Fe shell is not self-evident. The different lengths of the As-Fe scattering paths determined from the fit indicate that more than one binding form occur in parallel, although not necessary on the same Fe oxide phase. Shorter distances ranging from 2.7 to 2.9 Å are observed in many As-sorbed Fe oxides, in particular at low As coverage on ferrihydrite, which has a large number of exposed edges at its surface (in contrast to goethite). Such short scattering paths are commonly interpreted as bidentate mononuclear surface complexes ${}^2\text{E}$ (i.e., edge-sharing AsO_4 tetrahedra with $\text{Fe}(\text{O},\text{OH})_6$ octahedra) (Waychunas et al., 1993; Manceau, 1995; Fendorf et al., 1997; Marcus et al., 2004; Cancès et al., 2005). Because there are two different Fe oxide species present (goethite and ferrihydrite), the occurrence of two types of the ${}^2\text{E}$ surface complex seems plausible. Although their distances are quite similar and almost within the range of uncertainty given the limited k range, they are not the same because the fit results with just one of them were much worse. The longer distance of 3.57 Å suggests monodentate mononuclear bonds ${}^1\text{C}$ (i.e., single corner-sharing AsO_4 tetrahedra with $\text{Fe}(\text{O},\text{OH})_6$ octahedra). Fendorf et al. (1997) reported that at low surface coverage (i.e., $\log \Gamma < -2.27$), arsenate

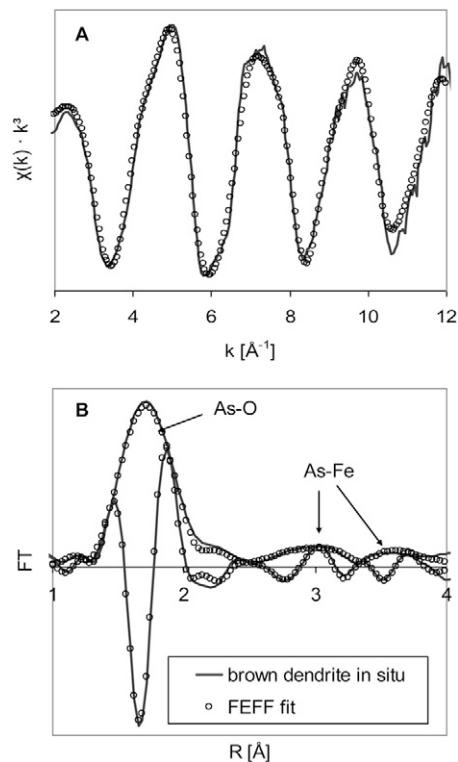


Fig. 5. Arsenic K-edge μ -extended X-ray absorption fine structure spectroscopy results of brown dendrite analyzed in situ with FEFF fit (circles) of the scorodite crystal structure model.

is sorbed onto goethite predominantly as a monodentate complex. Binuclear complexes (one AsO_4 tetrahedron attached at its corners to two $\text{Fe}(\text{O},\text{OH})_6$ octahedra, ${}^2\text{C}$) with path lengths of 3.2 to 3.4 Å have been found in many of the mentioned laboratory studies, in particular with As-sorbed goethite. The fit results of the present study with our natural samples, however, showed no significant contribution of ${}^2\text{C}$ complexes. Moreover, unlike with synthetic samples, the dominance of ${}^2\text{E}$ over the C complexes found in our experiments might be due to the presence of excess silica in the natural dendrite samples, as discussed in a previous study on natural Fe/Mn oxides (Marcus et al., 2004). Nonetheless, all in situ XAS analyses of the brown Fe-oxide dendrites indicate a similar trend in that the in situ As binding form in the limestone samples is a strong inner-spheric sorption of arsenate on the crystalline Fe-oxides ferrihydrite and goethite. They are not only the main dendrite-forming minerals but are also widespread Fe-oxide minerals in weathering environments. In fact, primary Fe-bearing mineral leaching and desilication yields these oxides as the only secondary soil-formed Fe-oxide minerals in temperate and cold climatic regions (McBride, 1994). These As hosts are therefore expected to remain stable when spread into soil concomitant with limestone amendment. Less clear is the fate of the adsorbed As when the soil becomes submerged and develops a moderately reducing environment of circum-neutral pH.

Mobility of Arsenic during Soil Incubation

Figure 6 shows the pH and redox conditions that developed in the water-saturated soil samples during incubation, together with the concentrations of “dissolved” (i.e., 0.2- μm filterable) Fe, total

Table 2. Parameters resulting from the FEFF fit of the As μ -extended X-ray absorption fine structure spectroscopy spectra derived for the brown limestone dendrites.

Scattering path	N	\AA^2	
		σ^2	R
As-O	4.0	0.0024 ± 0.001	1.67 ± 0.03
As-O-O-As	12.0	0.0024 ± 0.002	3.10 ± 0.06
As-Fe(1)	1.26	0.0090 ± 0.007	2.75 ± 0.05
As-Fe(2)	1.89	0.0095 ± 0.006	2.92 ± 0.04
As-Fe(3)	2.02	0.0092 ± 0.004	3.57 ± 0.03

As, and As(III) measured in soil pore water. All samples showed a gradual increase of pH and a decrease in Eh values until the third week of incubation, after which both values leveled off. The pH value was always a minimum of one unit higher, but the redox potential was always lower in the limed soil samples than in the untreated samples. The samples with moderate lime addition (10 g kg^{-1}) showed Eh values of 100 to 200 mV below those of the untreated samples. In the samples with high lime addition (100 g kg^{-1}), the difference was even greater (250–400 mV). Nonetheless, release of dissolved Fe and Mn was clearly controlled not only by the initiation of reducing conditions but also by the pH conditions because more Fe was mobilized in the soil without

added lime than in the limed samples. The experiments were not designed to investigate the amount and nature of any ferric oxide colloids, but it appears unlikely that development of anoxic conditions would increase the amount of such colloids, which may be hosting a fixed pool of As in soil pore water.

The results of the mobilization experiments show that As was mobilized at the onset of anoxic conditions but also in soil samples to which no lime had been added. The release of As showed no clear correlation with the release of Fe or Mn during the various incubations but rather gradually increased throughout the incubation period. In untreated soil samples, the total dissolved As concentration increased to $18 \pm 2.3 \mu\text{g L}^{-1}$ by Day 41, when the experiment was terminated. Such concentrations are common for uncontaminated soil pore water (Sadiq, 1997). The soil samples amended with pure CaCO_3 showed lower As concentrations after 41 d in comparison to the unamended soil samples, whereas those with lime additions showed higher As concentrations. These differences were significant (i.e., above error margins) only for the highest amendments of 100 g kg^{-1} (Fig. 6). The samples with high lime application (100 g kg^{-1}) produced the highest concentrations of released As ($25 \pm 2.5 \mu\text{g L}^{-1}$), with

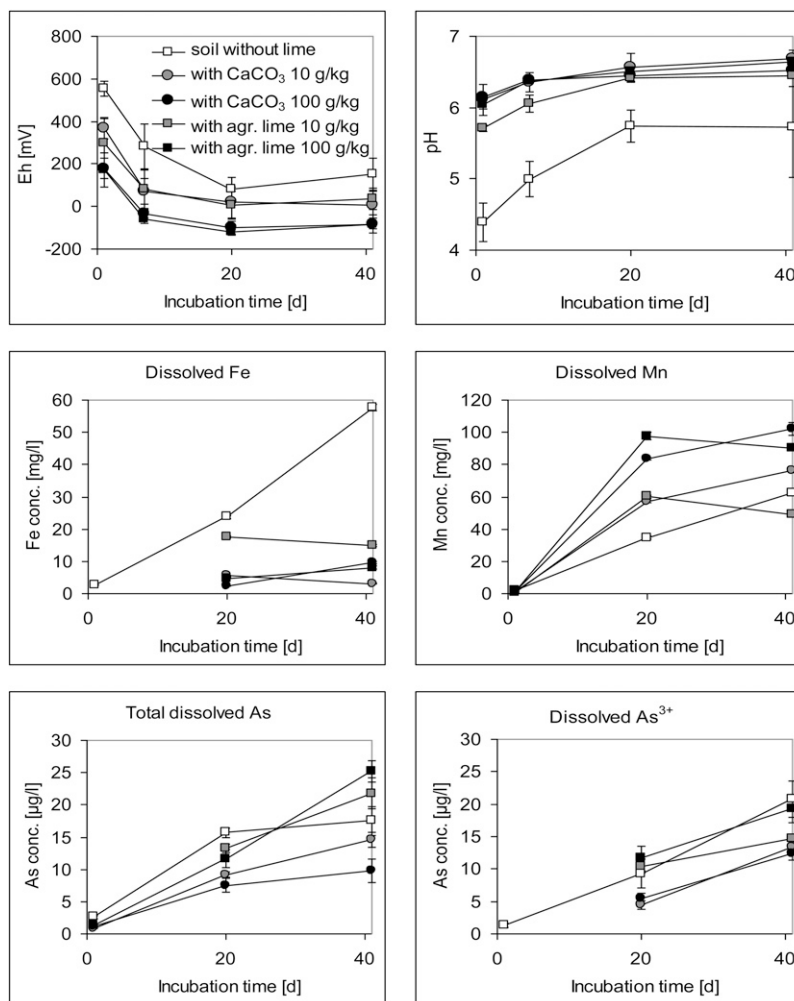


Fig. 6. Development of pH, redox potential (Eh), and dissolved concentrations of total As, Fe, Mn, and As(III) in soil pore water during the soil incubation experiments.

a relatively constant rate of $0.20 \pm 0.02 \mu\text{g As per kg (DW) lime-amended soil and day}$. When compared with unamended soil ($0.16 \pm 0.02 \mu\text{g kg}^{-1} \text{d}^{-1}$), the As release rate from the lime under these conditions is in the order of maximum $0.04 \mu\text{g kg}^{-1} \text{d}^{-1}$. The As present in the agricultural lime contributes to the total As pool available to mobilization, although not to the extent that could be expected based on its bulk concentration in the lime.

The leveling off in pH and Eh conditions at Day 20 does not imply that there are no further redox reactions taking place. In fact, a more complex feature of the As release dynamics appears when considering the As speciation in the soil pore water. The proportion of As(III) was around 50% of total As in the samples without added lime and with pure CaCO_3 amendment after 20 d and increased to 100% after 41 d. The untreated soil and the high-limestone samples reached an As(III) concentration of $21 \pm 2.8 \mu\text{g L}^{-1}$ by the end of the incubation. The samples treated with agricultural lime, in contrast, exhibited an arsenite fraction of 80 to 100% after 20 d, which decreased to about 70% after 41 d. The molar As/Fe ratio in the bulk soil was 4.0×10^{-4} , whereas in the pore water samples it was higher, ranging from 2.3×10^{-4} to 3.6×10^{-3} . This incongruent release is probably due to the dissolved species conversion from arsenate to arsenite. Such species-driven incongruent As release has also been found in rice paddy (Takahashi et al., 2004) and was explained by the weaker sorption of arsenite on Fe oxides under slightly acidic conditions (Masscheleyn et al., 1991; Reynolds et al., 1999; Takahashi et al., 2004).

The ambient physicochemical conditions were more effective in controlling the As species and concentrations released into pore water than the addition of different substances to the soil samples. The presence of excess lime may favor As immobilization as indicated by the experiments with pristine CaCO_3 additions. A potential As-removal mechanism is co-precipitation through the substitution $\text{CO}_3^{2-} \leftrightarrow \text{AsO}_3^{3-}$ and formation of $\text{Ca}(\text{CO}_3, \text{HAsO}_3)$ solid solution (Di Benedetto et al., 2006). Another As-removal mechanism is adsorption onto the calcite by formation of surface complexes (Cheng et al., 1999). A third one is precipitation of calcium arsenite or calcium arsenate, both having a relatively low solubility product. However, evaluation of solubility and stability of both the latter phases was conducted under a CO_2 -free atmosphere (Nishimura and Robins, 1998) because both phases are unstable under ambient environmental conditions (Magalhaes, 2002). Atmospheric carbon dioxide causes calcium arsenite and arsenate to decompose to calcium carbonate, whereas the As species released are scavenged by Fe oxides. Magnesium arsenate is affected by carbon dioxide in a similar manner (Magalhaes, 2002). The As removal is therefore due to adsorption onto the CaCO_3 rather than a precipitation mechanism. Nonetheless, As retention at the calcite surface is relatively weak compared with complexes at Fe-oxide surfaces. Therefore, in the mixed soil mineral systems, adsorption at calcite surfaces would not be expected to play a dominant role in the overall As retention unless amended at excess. Moreover, Fe oxide and lime treatment combinations were suggested to minimize As uptake by plants (Warren and Alloway, 2003).

Conclusions

We found no clear evidence of As release caused by liming even with limestone rich in As-bearing oxide dendrites. Even partial reductive dissolution of the dendrites does not necessarily lead to As release, at least not until their surface area becomes too small to repartition all the released As (Pedersen et al., 2006). Although the addition of agricultural lime did not effectively immobilize the As present in the soil in comparison with the pure CaCO_3 amendments, it did not cause an increased release of arsenite either. Dissolved arsenite in the pore water from soil treated with the agricultural lime was not found in significantly higher concentrations in comparison to unamended samples during the laboratory batch incubations under submerged conditions. Because arsenite is the highly mobile and toxic species, this finding in particular suggests a limited environmental hazard potential of the examined lime material. The relatively small effect of agricultural lime (compared with pure CaCO_3) supports the conclusion drawn from the results of the sequential extraction and XAS analyses (i.e., that As is predominantly bound in strong inner-sphere complexes with crystalline Fe oxides, which are not easily released under the conditions applied to the samples). The material used in our study is too extreme in oxide dendrite composition to be representative of the wealth of lime used for soil amendment. Nonetheless, it became clear that such dendrites may be prone with excessive As contents, and care should be taken if agricultural limestone is yellowish-brown colored.

Although apparently less harmful from a production agriculture standpoint, another important exposure pathway in assessing public health risks associated with As contamination is soil ingestion, either active ingestion by livestock or incidental ingestion by children. However, our analyses suggest that the arsenate in limestone is mainly bound to crystalline Fe oxides, and a recent study based on *in vitro* assays and speciation analysis has similarly demonstrated that the focus on total As content results in an overestimation of the risk posed by As when it is adsorbed to ferrihydrite (Beak et al., 2006). The sequential extraction results suggest that limestone and phosphate fertilizer amendment in parallel might lead to some As mobilization. However, phosphate in soil pore water becomes relatively low in the presence of excess Ca due to ageing of the inorganic fertilizer by phase transformation from dicalcium phosphate to less soluble octacalcium phosphate or hydroxylapatite-bound phosphate (see the review by Von Wandruszka, 2006). One may further argue against the application of As-bearing agricultural lime on areas where long-term anoxic conditions are to be expected on time scales beyond our laboratory experiments. In this context it is interesting to note that cattail and even rice plants have been found to be protected from As uptake by the formation of Fe oxide plaques on their roots (Keon-Blute et al., 2004; Liu et al., 2006). These plaques have been found to contain similar levels of As concentration as the limestone plaques of the present study.

Suggestions for quantitative As limits are beyond the scope of the present study. However, our As speciation results corroborate regulatory codes that set the permissible As content in agricultural lime relative to the respective Fe content, such as the 2007

California Fertilizing Materials Code (California Department of Food and Agriculture, 2007). The latter code, for example, states that agricultural mineral products shall not exceed 13 mg kg⁻¹ of As for each percent of iron (and manganese). Such a laboratory study is preliminary and has to be corroborated by more realistic field experiments involving application of phosphate and lime fertilizers in parallel. Nonetheless, we are confident that current and future research efforts in the development of improved regulations will consider the As/Fe ratio approach as more promising than simple absolute concentration thresholds for a comparative risk assessment.

Supplemental Information Available

Supplemental material is available and includes color figures showing the location of limestone and soil sampling sites, a plot showing interference effects on Hg-AAS measurements of As in sequential extraction solutions, the fit of the scorodite model to As EXAFS data, Fe and As XANES plots, and bulk powder diffraction patterns of black plaques and brown dendrites. This material is available free of charge at <http://jeq.scijournal.org>.

Acknowledgments

This work was funded through a grant from the German Science Foundation (GRK 826). Dr. B. Schulz-Dobrick helped with EPMA analyses, and Dr. H.D. Werner assisted with XRD. We thank HASYLAB (beamline A1) for granting us beamtime and Dr. E. Welter for help with the measurements. Assistance at ALS beamline 10.3.2 was provided by Dr. M. Marcus. The Advanced Light Source is supported by the Director, Office of Science, Office of Basic Energy Sciences, of the U.S. Department of Energy under Contract No. DE-AC02-05CH11231. We also thank the Associate Editor Dr. K.G. Karthikeyan for providing helpful reviews and comments.

References

ALA. 2008a. Online information given by the Agricultural Lime Association. Available at: <http://www.aglime.org.uk> (verified 17 June 2009).

ALA. 2008b. Lime calculator software provided by the Agricultural Lime Association. Available at: <http://www.aglime.org.uk> (verified 17 June 2009).

Aggett, J., and Y. Hayashi. 1987. Observations on the interference by copper(II), cobalt(II) and nickel(II) on the determination of arsenic by arsine generation atomic absorption spectrometry. *Analyst* 112:277–282.

Baur, W.H., and B.H. Onishi. 1969. Arsenic. p. A1–A33. In K.H. Wedepohl (ed.) *Handbook of geochemistry*. Springer-Verlag, Berlin, Germany.

Beak, D.G., N.T. Basta, K.G. Scheckel, and S.J. Traina. 2006. Bioaccessibility of arsenic(V) bound to ferrihydrite using a simulated gastrointestinal system. *Environ. Sci. Technol.* 40:1364–1370.

Berg, M., P.T.K. Trang, C. Stengel, J. Buschmann, P.H. Viet, N.V. Dan, W. Giger, and D. Stüben. 2008. Hydrological and sedimentary controls leading to arsenic contamination of groundwater in the Hanoi area, Vietnam: The impact of iron-arsenic ratios, peat, river bank deposits, and excessive groundwater abstraction. *Chem. Geol.* 249:91–112.

Cai, Y., J.C. Cabrera, M. Georgiadis, and K. Jayachandran. 2002. Assessment of arsenic mobility in the soils of some golf courses in South Florida. *Sci. Total Environ.* 291:123–134.

California Department of Food and Agriculture. 2007. Food and agricultural code division 7, chapter 5: Fertilizing materials. Available at: <http://www.cdffa.ca.gov/is/docs/Fertilizer%20Law%20and%20Regs.complete.rev.04.07.pdf> (verified 6 June 2009).

Cancès, B., F. Juillot, G. Morin, V. Laperche, L. Alvarez, O. Proux, J.-L. Hazemann, G.E. Brown, Jr., and G. Calas. 2005. XAS Evidence of As(V) association

with iron oxyhydroxides in a contaminated soil at a former arsenical pesticide processing plant. *Environ. Sci. Technol.* 39:9398–9405.

Charter, R.A., M.A. Tabatabai, and J.W. Schafer. 1995. Arsenic, molybdenum, selenium, and tungsten contents of fertilizers and phosphate rocks. *Commun. Soil Sci. Plant Anal.* 26:3051–3062.

Cheng, L.W., P. Fenter, N.C. Sturchio, Z. Zhong, and M.J. Bedzyk. 1999. X-ray standing wave study of arsenite incorporation at the calcite surface. *Geochim. Cosmochim. Acta* 63:3153–3157.

Di Benedetto, E., P. Costagliola, M. Benvenuti, P. Lattanzi, M. Romanelli, and G. Tanelli. 2006. Arsenic incorporation in natural calcite lattice: Evidence from electron spin echo spectroscopy. *Earth Planet. Sci. Lett.* 246:458–465.

Eiche, E., T. Neumann, M. Berg, B. Weinman, A. van Green, S. Norra, Z. Berner, P.T.K. Trang, P.H. Viet, and D. Stüben. 2008. Geochemical processes underlying a sharp contrast in groundwater arsenic concentrations in a village on the Red River delta, Vietnam. *Appl. Geochem.* 23:3143–3154.

Fendorf, S., M.J. Eick, P. Grossl, and D.L. Sparks. 1997. Arsenate and chromate retention mechanisms on goethite. 1. Surface structure. *Environ. Sci. Technol.* 31:315–320.

FGALI. 2008. Information given by the Federal German Association of the Lime Industry. Available at: <http://www.kalk.de> (verified 17 June 2009).

Gruebel, K.A., J.O. Leckie, and J.A. Davies. 1988. The feasibility of using sequential extraction techniques for arsenic and selenium in soils and sediments. *Soil Sci. Soc. Am. J.* 52:390–397.

Hudson-Edwards, K.A., S.L. Houghton, and A. Osborn. 2004. Extraction and analysis of arsenic in soils and sediments. *Trends Anal. Chem.* 23:745–752.

Jackson, B.P., and W.P. Miller. 2000. Effectiveness of phosphate and hydroxide for desorption of arsenic and selenium species from iron oxides. *Soil Sci. Soc. Am. J.* 64:1616–1622.

Keon, N.E., C.H. Swartz, D.J. Brabander, C. Harvey, and H.F. Hemond. 2001. Validation of an arsenic sequential extraction method for evaluating mobility in sediments. *Environ. Sci. Technol.* 35:2778–2784.

Keon-Blute, N., D.J. Brabander, H.F. Hemond, S.R. Sutton, M.G. Newville, and M.L. Rivers. 2004. Arsenic sequestration by ferric iron plaque on cattail roots. *Environ. Sci. Technol.* 38:6074–6077.

Kersten, M. 2001. Speciation of trace metals in sediments. p. 301–321. In A.M. Ure and C.M. Davidson (ed.) *Chemical speciation in the environment*, 2nd ed. Blackwell Science, Oxford, UK.

Kitahama, K., R. Kiriya, and Y. Baba. 1995. Refinement of the crystal structure of scorodite. *Acta Crystallogr. B* 31:322–324.

Liu, W.J., Y.G. Zhu, Y. Hu, P.N. Williams, A.G. Gault, A.A. Meharg, J.M. Charnock, and F.A. Smith. 2006. Arsenic sequestration in iron plaque, its accumulation and speciation in mature rice plants (*Oryza Sativa* L.). *Environ. Sci. Technol.* 40:5730–5736.

Magalhaes, M.C.F. 2002. Arsenic. An environmental problem limited by solubility. *Pure Appl. Chem.* 74:1843–1850.

Maity, S., S. Chakravarty, P. Thakur, K.K. Gupta, S. Bhattacharjee, and B.C. Roy. 2004. Evaluation and standardisation of a simple HG-AAS method for rapid speciation of As(III) and As(V) in some contaminated groundwater samples of West Bengal, India. *Chemosphere* 54:1199–1206.

Manceau, A. 1995. The mechanism of anion adsorption on iron oxides: Evidence for the bonding of arsenate tetrahedra on free Fe(O,OH)₆ edges. *Geochim. Cosmochim. Acta* 59:3647–3653.

Manceau, A., and W.P. Gates. 1997. Surface structural model for ferrihydrite. *Clays Clay Miner.* 45:448–460.

Manning, B.A., and S. Goldberg. 1996. Modeling competitive adsorption of arsenate with phosphate and molybdate on oxide minerals. *Soil Sci. Soc. Am. J.* 60:121–131.

Marcus, M.A., A. Manceau, and M. Kersten. 2004. Mn, Fe, Zn and As speciation in a fast-growing ferromanganese marine nodule. *Geochim. Cosmochim. Acta* 68:3125–3136.

Masscheleyn, P.H., R.D. Delaune, and W.H. Patrick. 1991. Effect of redox potential and pH on arsenic speciation and solubility in a contaminated soil. *Environ. Sci. Technol.* 25:1414–1419.

McBride, M.B. 1994. *Environmental Chemistry of Soils*. Oxford Univ. Press, Oxford, UK.

McBride, M.B., and G. Spiers. 2001. Trace element content of selected fertilizers and dairy manures as determined by ICP-MS. *Commun. Soil Sci. Plant Anal.* 32:139–156.

McCleskey, R.B., D.K. Nordstrom, and A.S. Maest. 2004. Preservation of water samples for arsenic (III/V) determinations: An evaluation of literature and new analytical results. *Appl. Geochem.* 19:995–1009.

- McKeown, D.A., and J.E. Post. 2001. Characterization of manganese oxide mineralogy in rock varnish and dendrites using X-ray absorption spectroscopy. *Am. Mineral.* 86:701–713.
- Näykki, T., P. Perämäki, J. Kyjala, and A. Mikkonen. 2001. Optimization of a flow injection hydride generation atomic absorption spectrometric method for the determination of arsenic, antimony and selenium in iron chloride/sulfate-based water treatment chemical. *Anal. Chim. Acta* 439:229–238.
- Ngoc, K.C., N.V. Nguyen, B.N. Dinh, S.L. Thanh, S. Tanaka, Y. Kang, K. Sakurai, and K. Iwasaki. 2009. Arsenic and heavy metal concentrations in agricultural soils around tin and tungsten mines in the Dai Tu district, N. Vietnam. *Water Air Soil Pollut.* 197:75–89.
- Nishimura, T., and R.G. Robins. 1998. A re-evaluation of the solubility and stability regions of calcium arsenites and calcium arsenates in aqueous solution at 25°C. *Min. Process. Extract. Metal. Rev.* 18:283–308.
- Okrusch, H., J.A. Lorenz, and S. Weyer. 2007. The genesis of sulfide assemblages in the former wilhelm mine, Spessart, Bavaria, Germany. *Can. Mineral.* 45:723–750.
- Pedersen, H.D., D. Postma, and R. Jakobsen. 2006. Release of arsenic associated with the reduction and transformation of iron oxides. *Geochim. Cosmochim. Acta* 70:4116–4129.
- Pigna, M., G.S.R. Krishnamurti, and A. Violante. 2006. Kinetics of arsenate sorption-desorption from metal oxides: Effect of residence time. *Soil Sci. Soc. Am. J.* 70:2017–2027.
- Price, R.E., and T. Pichler. 2006. Abundance and mineralogical association of arsenic in the Suwannee limestone (Florida): Implications for arsenic release during water-rock interaction. *Chem. Geol.* 228:44–56.
- Ravel, B., and M. Newville. 2005. ATHENA, ARTEMIS, HEPHAESTUS: Data analysis for X-ray absorption spectroscopy using IFEFFIT. *J. Synchrotron Radiat.* 12:537–541.
- Raven, K.P., and R.H. Loeppert. 1997. Trace element composition of fertilizers and soil amendments. *J. Environ. Qual.* 26:551–557.
- Rehr, J.J., and R.C. Albers. 2000. Theoretical approaches to x-ray absorption fine structure. *Rev. Mod. Phys.* 72:621–654.
- Ressler, T. 1998. WinXAS: A program for x-ray absorption spectroscopy data analysis under MS-Windows. *J. Synchrotron Radiat.* 5:118–122.
- Reynolds, J.G., D.V. Naylor, and S.E. Fendorf. 1999. Arsenic sorption in phosphate-amended soils during flooding and subsequent aeration. *Soil Sci. Soc. Am. J.* 63:1149–1156.
- Ryan, J.N., and P.M. Gschwend. 1991. Extraction of iron oxides from sediments using reductive dissolution by titanium (III). *Clays Clay Miner.* 39:509–518.
- Sadiq, M. 1997. Arsenic chemistry in soils: An overview of thermodynamic predictions and field observations. *Water Air Soil Pollut.* 93:117–136.
- Sherman, D.M., and S.R. Randall. 2003. Surface complexation of arsenic(V) to iron(III) (hydr)oxides: Structural mechanism from ab initio molecular geometries and EXAFS spectroscopy. *Geochim. Cosmochim. Acta* 67:4223–4230.
- Schmitt, R.T. 2001. Zur petrographie, geochemie und buntmetallmineralisation des zechstein 1 (Werra-Folge) im gebiet Huckelheim- Großkahl (Nordwestlicher Spessart). *Naturwissenschaftlicher Verein: Aschaffenburg, Vol. 20 (in German).*
- Takahashi, Y., R. Minamikawa, K.H. Hattori, K. Kurishima, N. Kihou, and K. Yuita. 2004. Arsenic behavior in paddy fields during the cycle of flooded and non-flooded periods. *Environ. Sci. Technol.* 38:1038–1044.
- VDLUFA. 1991. Handbook on methods Vol. I: The investigation of soils. (In German). VDLUFA-Verlag, Darmstadt, Germany.
- Von Wandruszka, R. 2006. Phosphorus retention in calcareous soils and the effect of organic matter on its mobility. *Geochem. Trans.* 7:6. doi: 10.1186/1467-4866-7-6.
- Warren, G.P., and B.J. Alloway. 2003. Reduction of arsenic uptake by lettuce with ferrous sulfate applied to contaminated soil. *J. Environ. Qual.* 32:767–772.
- Waychunas, G.A., B.A. Rea, C.C. Fuller, and J.A. Davis. 1993. Surface chemistry of ferrihydrite: Part 1. EXAFS studies of the geometry of coprecipitated and adsorbed arsenate. *Geochim. Cosmochim. Acta* 57:2251–2269.